Communications of BAO, Vol. 73, Issue 2, 2026, pp. 339-345

Compact Planetary Nebulae as Laboratories of an Unstable Universe

Ş. Yalgın *

Ankara University, Institute of Science, Department of Astronomy and Space Sciences, 06110, Ankara, Türkiye

Abstract

Planetary nebulae provide a direct view of stellar matter in transit from stars to the interstellar medium, capturing stellar evolution in the act of Galactic recycling. Originating from low- and intermediate-mass stars, they constitute an important source of chemically enriched gas and dust in the Galaxy. While their progenitor stars evolve over timescales of millions to billions of years, the planetary nebula phase remains observable for only a few tens of thousands of years. As the central star evolves toward higher temperatures, the ionization structure, density distribution, and dust properties of the nebula respond to a continuously changing radiation field. Their rapidly evolving nature makes planetary nebulae powerful tracers of the dynamic Universe. We investigate a sample of 18 well-characterized compact planetary nebulae, focusing on their dust properties and evolutionary status using published photoionization models. By combining published optical, infrared, and radio observations with model inputs, we reconstruct their spectral energy distributions without refitting and examine the gas and dust properties in relation to stellar mass loss and the recycling of matter into the interstellar medium. Finally, we discuss the implications of the derived gas and dust properties for the planetary nebula missing-mass problem.

Keywords: *planetary nebulae; dust temperature; mass loss; stellar evolution*

1. Introduction

Planetary nebulae (PNe) reveal the evolution of circumstellar material following the asymptotic giant branch (AGB) phase. During AGB evolution, mixing processes alter the chemical composition of the stellar envelope, and stellar winds carry this processed material into the surrounding medium, contributing to Galactic chemical enrichment. The subsequent PN phase remains observable for only a few tens of thousands of years (Jacob et al., 2013). Over this interval, changes in the central star's radiation field and stellar wind influence the ionization conditions and physical structure of the expanding nebula (Kwok, 2024).

The observed emission of a PN arises from several components that require complementary observational constraints. Optical spectra provide diagnostics of the ionized gas, while radio continuum and infrared measurements constrain free–free emission and thermal dust emission, respectively (Planck Collaboration et al., 2015). Dust also influences the thermal balance of the gas through photoelectric heating, linking its properties to the nebular emission spectrum (Stasińska & Szczerba, 1999, Weingartner & Draine, 2001, van Hoof et al., 2004). Combining observations across these wavelength ranges therefore helps constrain the gas and dust within a common physical framework. Photoionization modelling provides a means of relating these observations to the properties of the central star and its surrounding material. Previous applications have combined emission-line measurements, infrared and radio fluxes, and angular dimensions to constrain stellar and nebular parameters (van Hoof & van de Steene, 1999). Detailed studies of compact PNe have also demonstrated the value of jointly modelling optical and infrared observations to investigate their gas and dust components (Bandyopadhyay et al., 2021). Spectroscopic and photoionization analyses by Aksaker et al. (2024), Yalgın et al. (2025), and Aksaker et al. (2026) provide a basis for the comparative investigation presented here.

The nebular mass budget offers an additional perspective on stellar mass loss. CO observations indicate that the circumstellar envelopes of some AGB stars contain more than 1 $M_{\odot}$, whereas typical planetary

*sengulyalgin@gmail.com

nebular masses are around 0.2 $M_{\odot}$ (Kwok, 2024). This comparison raises the question of how much of the material expelled during AGB evolution is subsequently accounted for in the observed nebula, providing a context for the planetary nebula missing-mass problem (Kimura et al., 2012, Santander-García et al., 2022, Wareing et al., 2007). A substantial amount of material may reside in neutral atomic and molecular gas, so the ionized component alone may not represent the full nebular mass budget (Volk & Kwok, 1997). In this study, we assess how the ionized gas masses derived for 18 compact planetary nebulae compare with the estimated masses lost by their progenitor stars, with a discussion of the limitations of the ionized component in accounting for the expelled material.

2. Sample and Parameters

The sample comprises 18 compact PNe selected on the basis of their shared observational origin and the availability of published photoionization analyses by Aksaker et al. (2024), Yalgın et al. (2025) and Aksaker et al. (2026). Their optical spectra were obtained with RTT150/TFOSC at the TÜBİTAK National Observatory. The availability of central-star effective temperatures and luminosities also permits a comparative examination of their positions relative to post-AGB evolutionary tracks.

The emission-line measurements, elemental and grain abundances, stellar and nebular model parameters, and infrared and radio measurements were compiled from these studies. We reconstructed the spectral energy distributions with CLOUDY (Chatzikos et al., 2023) using the published inputs without modification or refitting (Fig.1). Dust temperatures ($T_{\rm dust}$) and ionized nebular masses were obtained from these calculations. The ionized masses reproduce those reported in Yalgın (2026) for 16 objects and in Aksaker et al. (2026) for PN G041.8+04.4 and PN G077.7+03.1.

The contribution of the present work is a sample-wide comparison that brings these previously published results into a common analysis. We compare the elemental abundance distributions with Galactic reference values (Fig.2), place all 18 central stars on a common Hertzsprung–Russell diagram with post-AGB evolutionary tracks (Fig.3), and present the reconstructed SEDs together. We examine the relationship between $T_{\rm dust}$ and model inner radius ($R_{\rm in}$) for all 18 objects and compare the ionized-to-ejected mass fraction, defined as $f_{\rm ion} = 100\,M_{\rm ion}/(M_i - M_f)$ in percent, with the published evolutionary ages of the 16 objects with numerical age estimates. Here, $M_{\rm ion}$ is the ionized gas mass, while M_i and M_f are the initial and final stellar masses, respectively.

3. Discussion

Figure 4 examines two complementary aspects of the sample: the distribution of $T_{\rm dust}$ with $R_{\rm in}$ for all 18 objects, and $f_{\rm ion}$ as a function of evolutionary age for the 16 objects with published numerical ages. PN G050.4-01.6 and PN G095.2+25.4 are retained in the structural comparison but excluded from the age analysis because numerical ages were not reported in Aksaker et al. (2024).

Panel (a) (Fig.4) shows a weak negative rank correlation between $R_{\rm in}$ and $T_{\rm dust}$, which is not statistically significant ($\rho_{\rm S} = -0.318$, $p = 0.198$). Although the two objects with the largest inner radii are also the coolest, substantial temperature differences occur among objects with similar $R_{\rm in}$. The sample, therefore, does not establish a simple temperature sequence with increasing $R_{\rm in}$. This scatter is compatible with the dependence of dust heating on stellar illumination, grain properties, and the local radiation field. The interpretation of dust properties as indicators of nebular evolution consequently requires more than a single geometrical parameter (Stasińska & Szczerba, 1999). In particular, the adopted $R_{\rm in}$ describes the inner boundary of the model gas distribution and is not treated here as a direct evolutionary clock.

Panel (b) (Fig.4) reveals a strong positive rank correlation ($\rho_{\rm S} = 0.806$, $p = 1.64 \times 10^{-4}$) between evolutionary age and $f_{\rm ion}$. Thus, objects with larger evolutionary ages generally have a greater fraction of their estimated expelled mass represented by ionized gas. It is qualitatively consistent with the progressive ionization of circumstellar material, a picture supported by comparisons of ionic, atomic, and molecular components in PNe at different evolutionary stages (Bernard-Salas & Tielens, 2005).

Nevertheless, this cross-sectional comparison does not directly measure the growth of ionized mass in individual nebulae. The plotted quantity is a ratio, and its behaviour can reflect differences in both ionized mass and estimated ejected mass. Furthermore, the evolutionary ages and progenitor mass estimates share dependencies on the adopted stellar parameters and evolutionary tracks (Miller Bertolami, 2016). The correlation should therefore be interpreted as an association within the compiled sample, rather than a

doi: https://doi.org/10.52526/25792776-26.73.2-339

calibrated relation describing a universal time evolution. The reported significance is based on the nominal parameter values and does not incorporate their uncertainties.

For the full sample, $f_{\rm ion}$ spans approximately 1.45×10^{-4}–3.49 per cent, with a median of 0.097 per cent (Table 1). Fourteen of the 18 objects have fractions below one per cent. The age subsample has a higher median of 0.257 per cent, partly because the two omitted objects have low ionized fractions. These results indicate that the modelled ionized component accounts for only a small part of the estimated evolutionary mass loss, irrespective of the presence of an age association.

This comparison requires a distinction between integrated stellar mass loss and the mass of the presently modelled nebula. Where the ejected mass is estimated as the difference between initial and final stellar masses, it need not correspond exclusively to the material forming the currently visible PN shell. Likewise, the ionized gas does not represent the complete circumstellar inventory. Neutral atomic and molecular regions can contain additional material (Bernard-Salas & Tielens, 2005, Kwok, 2024), while molecular mass estimates depend on the chemical assumptions used to convert observed tracers into total gas masses (Kimura et al., 2012). Material may also be distributed outside the bright central nebula. Faint ionized haloes preserve evidence of earlier AGB mass loss (Corradi et al., 2003), while hydrodynamical calculations show that interaction with the interstellar medium can displace AGB ejecta into downstream structures (Villaver et al., 2003, Wareing et al., 2007). These mechanisms offer possible explanations for the difference between the estimated expelled mass and the modelled ionized mass, but their individual contributions cannot be established from the present figure. Moreover, including observed molecular gas does not necessarily close the mass budget in every system (Santander-García et al., 2022). The present analysis cannot distinguish the relative contributions of these effects.

The principal result is therefore twofold: the ionized component represents a small fraction of the estimated expelled material, and this fraction is positively associated with the reported evolutionary ages in the available subsample. Observations of the neutral and molecular components are needed to assess whether the trend reflects changes in the ionized share of the nebular gas.

4. Conclusions

We assembled published observational measurements and model inputs for 18 compact planetary nebulae sharing a common RTT150/TFOSC observational basis. Using the original inputs without refitting, we reconstructed their spectral energy distributions with CLOUDY and obtained $T_{\rm dust}$ and $M_{\rm ion}$. These results were examined alongside the published elemental abundances and evolutionary estimates.

$T_{\rm dust}$ shows no statistically significant correlation with $R_{\rm in}$. For the 16 objects with published numerical evolutionary ages, the ionized fraction exhibits a strong positive rank correlation with age ($\rho_{\rm S} = 0.806$, $p = 1.64 \times 10^{-4}$). Its interpretation requires consideration of parameter uncertainties and the shared dependence of the ages and ejected-mass estimates on stellar evolutionary models.

The modelled ionized gas accounts for only a small fraction of the estimated integrated evolutionary mass loss in this sample. Extending the existing photoionization models to include surrounding neutral and molecular material, together with observations of extended circumstellar structures, would enable a more complete assessment of the mass budget. Such studies could help clarify the relationship between the material traced by the visible nebula and the broader mass-loss history of its progenitor.

Table 1. Parameters of the 18 compact PNe. The ionized-to-ejected mass fraction is $f_{\rm ion} = 100\,M_{\rm ion}/M_{\rm ej}$ in per cent, where $M_{\rm ej} = M_i - M_f$. Dashes indicate unavailable numerical evolutionary ages.

PN designation	$R_{\rm in}$ (pc)	$T_{\rm dust}$ (K)	Age (yr)	M_f ($M_\odot$)	$M_{\rm ej}$ ($M_\odot$)	$M_{\rm ion}$ ($M_\odot$)	$f_{\rm ion}$ (%)
PN G019.8+05.6	0.031	117	339	0.690	2.510	9.900×10^{-5}	0.003944
PN G021.3+02.2	0.060	100	742	0.640	2.160	1.161×10^{-3}	0.053750
PN G034.5-11.7	0.012	200	22073	0.530	0.470	1.267×10^{-2}	2.695745
PN G048.5+04.2	0.036	95	33905	0.510	0.290	7.391×10^{-3}	2.548621
PN G050.4-01.6	0.013	113	—	0.920	3.580	2.252×10^{-3}	0.062905
PN G080.2+03.8	0.030	266	2555	0.640	2.160	2.840×10^{-3}	0.131481
PN G095.2+25.4	0.013	116	—	0.920	3.580	5.200×10^{-6}	0.000145
PN G135.9+55.9	0.103	174	121	0.640	2.160	2.100×10^{-5}	0.000972
PN G153.7-01.4	0.183	75	1664	0.580	1.420	3.397×10^{-2}	2.392254
PN G183.0+00.0	0.222	67	11346	0.570	0.630	2.197×10^{-2}	3.487302
PN G202.9+07.4	0.076	131	249	0.710	2.590	1.170×10^{-4}	0.004517
PN G216.9-05.2	0.060	151	214	0.660	2.340	3.900×10^{-4}	0.016667
PN G021.2+02.9	0.096	141	324	0.658	2.342	1.020×10^{-3}	0.043553
PN G048.8+08.4	0.026	160	4835	0.562	0.688	8.400×10^{-5}	0.012209
PN G059.8-00.5	0.051	144	3042	0.576	0.924	7.100×10^{-3}	0.768398
PN G063.0+00.5	0.116	119	1647	0.581	1.419	5.430×10^{-3}	0.382664
PN G041.8+04.4	0.080	130	7100	0.528	0.472	4.350×10^{-3}	0.921610
PN G077.7+03.1	0.059	145	600	0.619	1.881	8.080×10^{-3}	0.429559

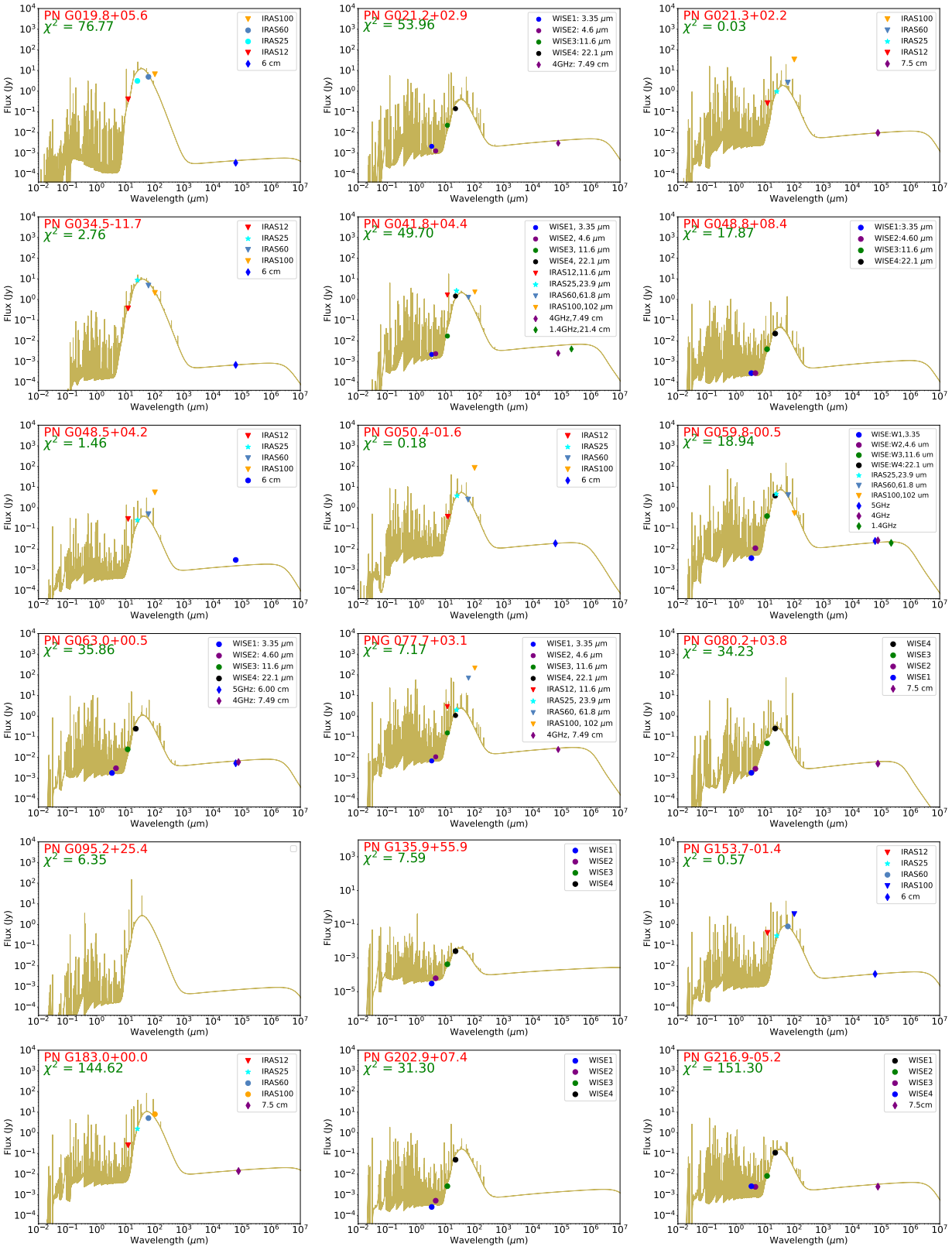

Figure 1. Spectral energy distributions of the 18 compact PNe reconstructed with CLOUDY using published model inputs without refitting. Symbols show WISE, IRAS, and radio flux measurements where available; triangles indicate upper limits.

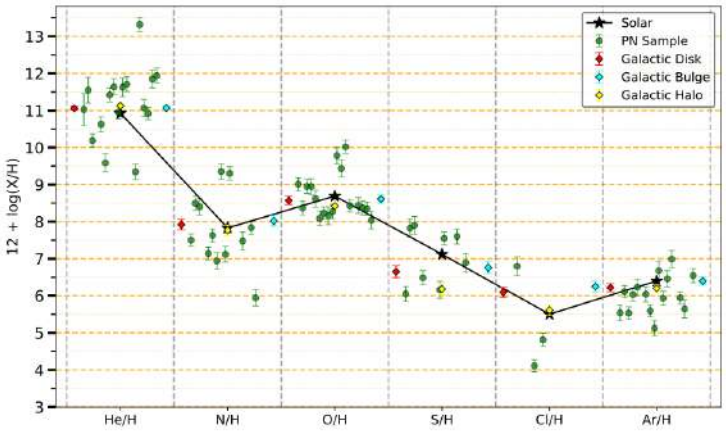

Figure 2. Elemental abundances of the 18 PNe, expressed as $12 + \log(X/H)$, compared with Galactic bulge, disk, and halo PN means from Kwitter & Henry (2022) and solar values from Asplund et al. (2009) (solid line). Galactic abundance uncertainties are from Rodríguez (2020).

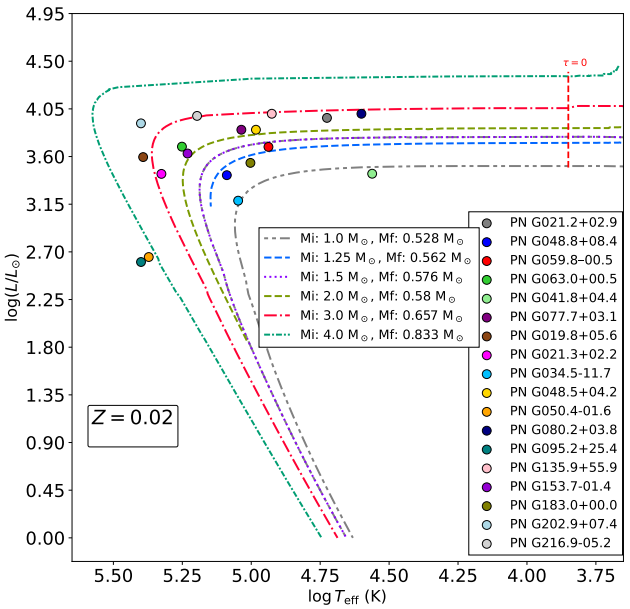

Figure 3. H–R diagram of the 18 PN central stars with post-AGB evolutionary tracks from Miller Bertolami (2016). The red dashed line marks the adopted post-AGB onset at $\log T_{\rm eff} = 3.85$.

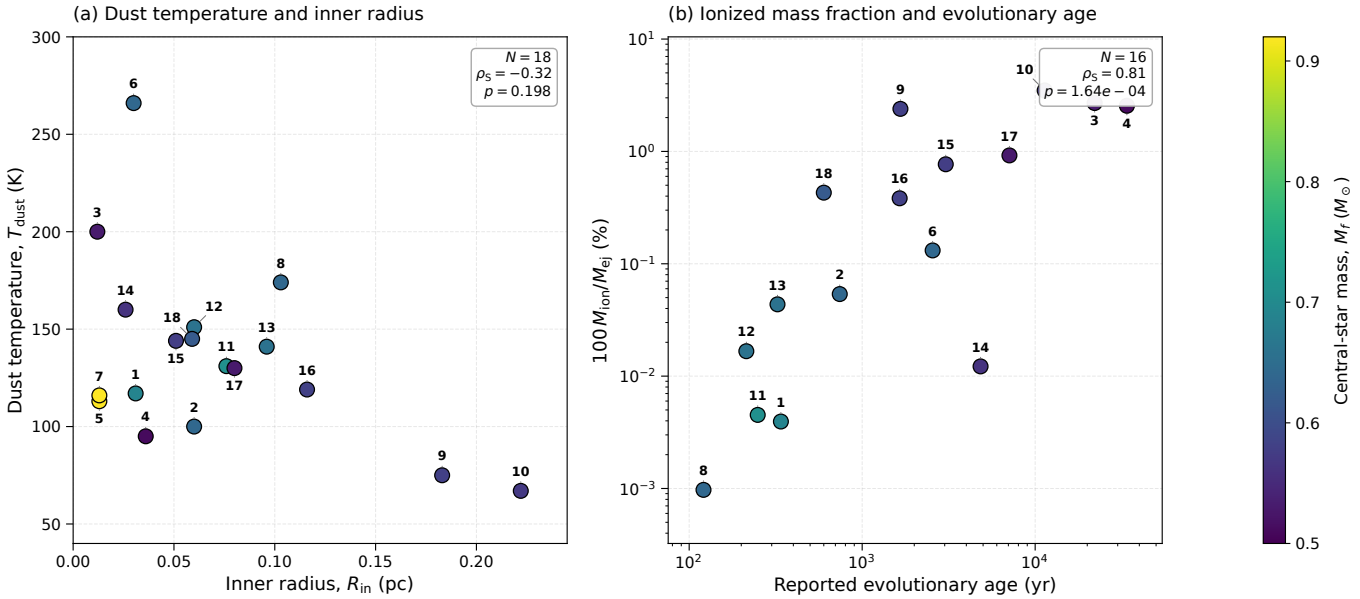

1. PN G019.8+05.6
2. PN G021.3+02.2
3. PN G034.5-11.7
4. PN G048.5+04.2
5. PN G050.4-01.6 *
6. PN G080.2+03.8
7. PN G095.2+25.4 *
8. PN G135.9+55.9
9. PN G153.7-01.4
10. PN G183.0+00.0
11. PN G202.9+07.4
12. PN G216.9-05.2
13. PN G021.2+02.9
14. PN G048.8+08.4
15. PN G059.8-00.5
16. PN G063.0+00.5
17. PN G041.8+04.4
18. PN G077.7+03.1

Figure 4. (a) Dust temperature versus inner radius for all 18 PNe. (b) Ionized-to-ejected mass fraction, $100\,M_{\rm ion}/M_{\rm ej}$, versus reported evolutionary age for the 16 objects with published numerical ages, where $M_{\rm ej} = M_i - M_f$. Colours indicate central-star mass, and numbers identify the objects listed below the panels. Objects marked with an asterisk have no published numerical ages and appear only in panel (a). Spearman rank coefficients and p-values are shown in each panel.

References

Aksaker N., Erzincan N., Akyuz A., Temiz U., 2024, Acta Astronomica, 74, 201

Aksaker N., Yalgın Ş., Erzincan N., Akyuz A., 2026, Mon. Not. R. Astron. Soc. , 549, stag892

Asplund M., Grevesse N., Sauval A. J., Scott P., 2009, Ann. Rev. Astron. Astrophys. , 47, 481

Bandyopadhyay R., Das R., Mondal S., 2021, Mon. Not. R. Astron. Soc. , 504, 816

Bernard-Salas J., Tielens A. G. G. M., 2005, Astron. Astrophys. , 431, 523

Chatzikos M., et al., 2023, Rev. Mex. Astron. Astrofis. , 59, 327

Corradi R. L. M., Schönberner D., Steffen M., Perinotto M., 2003, Mon. Not. R. Astron. Soc. , 340, 417

Jacob R., Schönberner D., Steffen M., 2013, Astron. Astrophys. , 558, A78

Kimura R. K., Gruenwald R., Aleman I., 2012, Astron. Astrophys. , 541, A112

Kwitter K. B., Henry R. B. C., 2022, Publ. Astron. Soc. Pac. , 134, 022001

Kwok S., 2024, Galaxies, 12, 39

Miller Bertolami M. M., 2016, Astron. Astrophys. , 588, A25

Planck Collaboration et al., 2015, Astron. Astrophys. , 573, A6

Rodríguez M., 2020, Mon. Not. R. Astron. Soc. , 495, 1016

Santander-García M., Jones D., Alcolea J., Bujarrabal V., Wesson R., 2022, Astron. Astrophys. , 658, A17

Stanghellini L., García-Hernández D. A., García-Lario P., Davies J. E., Shaw R. A., Villaver E., Manchado A., Perea-Calderón J. V., 2012, Astrophys. J. , 753, 172

Stasińska G., Szczerba R., 1999, Astron. Astrophys. , 352, 297

Villaver E., García-Segura G., Manchado A., 2003, Astrophys. J. Lett. , 585, L49

Volk K., Kwok S., 1997, Astrophys. J. , 477, 722

Wareing C. J., Zijlstra A. A., O'Brien T. J., 2007, Mon. Not. R. Astron. Soc. , 382, 1233

Weingartner J. C., Draine B. T., 2001, Astrophys. J. Suppl. Ser. , 134, 263

Yalgın Ş., 2026, in Chemin Y.-H., ed., , Planetary Science – Explorations, Missions, and Mapping. IntechOpen

Yalgın Ş., Aksaker N., Erzincan N., Akyuz A., 2025, New Astronomy, 119, 102413

van Hoof P. A. M., van de Steene G. C., 1999, Mon. Not. R. Astron. Soc. , 308, 623

van Hoof P. A. M., Weingartner J. C., Martin P. G., Volk K., Ferland G. J., 2004, Mon. Not. R. Astron. Soc. , 350, 1330